

# Paying Attention to Activation Maps in Camera Pose Regression

Yoli Shavit

Ron Ferens

Yosi Keller

Bar-Ilan University, Israel

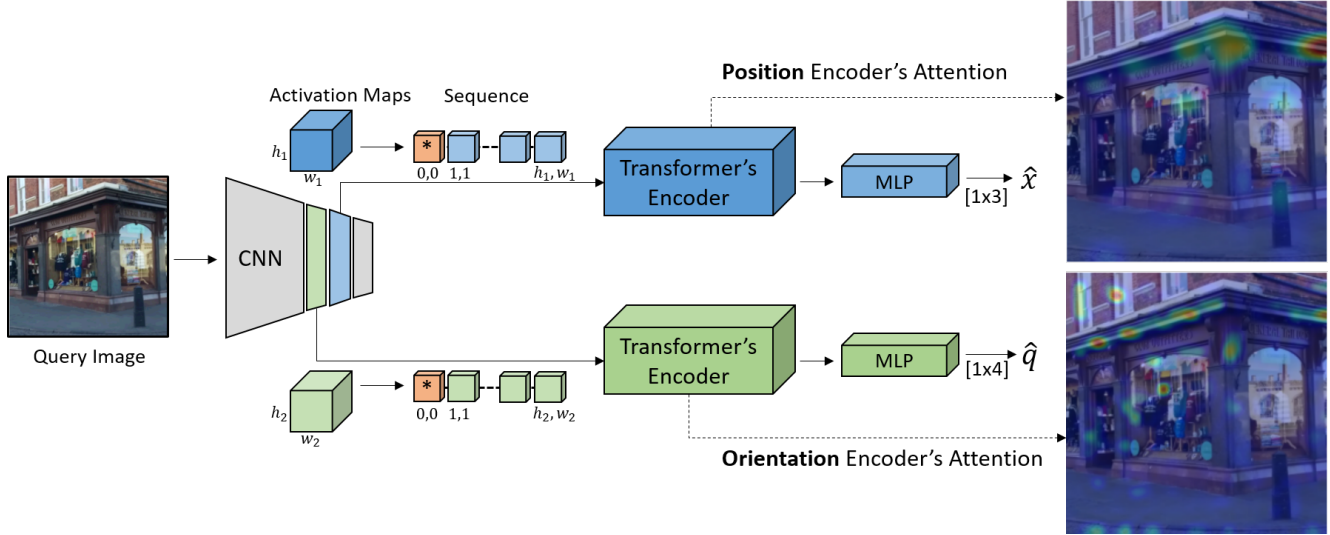


**Figure 1:** The proposed attention-based regression localization scheme. The input image is first encoded by a convolutional backbone. Two activation maps, at different resolutions, are transformed into sequential representations. The two activation sequences are analyzed by dual Transformer encoders, one per regression task. We depict the attention weights via heatmaps. Position is best estimated by corner-like image features, while orientation is estimated by edge-like features. Each Transformer encoder output is used to regress the respective camera pose component (position  $\hat{x}$  or orientation  $\hat{q}$ ).

## Abstract

Camera pose regression methods apply a single forward pass to the query image to estimate the camera pose. As such, they offer a fast and light-weight alternative to traditional localization schemes based on image retrieval. Pose regression approaches simultaneously learn two regression tasks, aiming to jointly estimate the camera position and orientation using a single embedding vector computed by a convolutional backbone. We propose an attention-based approach for pose regression, where the convolutional activation maps are used as sequential inputs. Transformers are applied to encode the sequential activation maps as latent vectors, used for camera pose regression. This allows us to pay attention to spatially-varying deep features. Using two Transformer heads, we separately focus on the features for camera position and orientation, based on how informative they are per task. Our proposed approach is shown to compare favorably to contemporary pose regressors schemes and achieves state-of-the-art accuracy across multiple out-

door and indoor benchmarks. In particular, to the best of our knowledge, our approach is the only method to attain sub-meter average accuracy across outdoor scenes. We make our code publicly available from: [here](#).

## 1. Introduction

Estimating the camera position and orientation using a captured image is an essential task in various contemporary computer vision applications, ranging from augmented reality to autonomous driving to navigation in closed environments such as malls, museums, airports and amusement parks, to name a few. Many of these applications require a fast and light-weight solution that is deployable on low-end devices, such as cellphones.

Recent *state-of-the-art* pipelines for visual pose estimation follow a hierarchical paradigm [28, 32, 26], where given a query image, an image retrieval (IR) method is first applied to fetch candidate images from a large, geo-referenced image database. Local features are ex-

tracted from the query and geo-referenced images and then matched. The resulting 2D-2D matches are transformed into 2D-3D correspondences using depth and/or a 3D model obtained with methods such as Light Detection and Ranging (LiDAR) and Structure from Motion (SfM). Finally, the pose (or a set of poses) is estimated from 2D-3D matches using Perspective-n-Point (PnP) and RANSAC algorithms [11]. While recent pipelines implementing the aforementioned approach achieve remarkable accuracy, they entail significant difficulties. First, such systems have to be implemented in a client-server architecture, due to the large image datasets that cannot be stored on thin clients (cellphone etc.). Second, a client-server approach requires an online data connection which is inapplicable for standalone localization applications. Last, the localization typically requires 50 – 2000ms processing time, depending on the method used, the size of the database and the number of matches [26]. In contrast, absolute regression-based approaches estimate the camera pose with a single forward pass, using the query image as an input to a trained regressor. The end device has to store only the regressor parameters.

As convolutional neural networks (CNNs) were shown to be efficient and accurate regressors in multiple domains, they were also applied to camera pose regression, starting with the seminal work of Kendall et al. [16]. The proposed architecture consisted of a convolutional backbone and a multilayer perceptron (MLP) head, separately regressing the position and orientation. The appealing 5 ms runtime and simplicity (a single component instead of a heavy pipeline) paved the way to a new research paradigm for camera pose estimation. Numerous methods, soon to follow, aimed at maintaining the low runtime and memory requirements, while improving the accuracy and generalization of the original method [16, 14, 15, 20, 21, 36, 38, 31, 37, 6].

Different camera pose regressors suggested different backbones [20, 31], loss formulations [15] and MLP architectures [38, 21] as well as additional manipulations of the output [36, 37]. Common to all these methods, is that they apply the pose regression using a *single* global image encoding computed by the backbone CNN.

In this work, we propose a novel attention-based approach that considers an activation map as a sequence of local spatial embeddings. Specifically, we employ Transformers [35], shown to provide an efficient computational means for analyzing spatially varying image activations as sequences [7]. This allows for an adaptive analysis of the spatial image content, as images typically contain a mixture of localization-informative and uninformative image cues. Thus, we cast the camera pose regression as two sequence-to-one problems, where the intermediate activation maps are input to a pair of translation-aware and rotation-aware Transformer encoders (Fig. 1). The output of each encoder

is used to regress the corresponding localization attribute. The gist of our approach is that each Transformer Encoder captures different informative image cues for either position or orientation estimation. We demonstrate this by overlaying the attention weights as heatmaps (Figs. 1 and 3). The largest attention values of the Positional Encoder are around corners, which are a commonly used localization cue, as in the SIFT detector [18]. Similarly, the Orientational Encoder emphasizes elongated edges that are informative visual cues for orientation estimation. Other image features that are less location-informative show weak attention activations. By adaptively detecting and weighting the informative spatial activations, Encoders improve the localization accuracy.

In summary, our contributions are as follows:

- We propose a novel attention-based approach to camera pose regression using dual encoders, one per regression task.
- Our approach is experimentally shown to compare favourably with *state-of-the-art* regression-based schemes, when applied to outdoor and indoor localization datasets.

## 2. Related Work

### 2.1. Image-Based Camera Pose Estimation

A common approach to image-based pose estimation applies large-scale image retrieval followed by image matching and PnP-RANSAC [32, 26, 22, 10]. Each query image to be localized, is encoded using a CNN trained for IR, and a relatively small set of nearest neighbors is retrieved for image-to-image matching. Local feature matching can be applied using brute force methods [32] or another learned component [27]. In order to convert image matches to the world plane, spatial information needs to be available at inference time. The pose can then be estimated using PnP-RANSAC from 2D-3D correspondences. In this work we study a faster and lighter alternative to this pipelined approach, namely camera pose regression.

Camera pose regression was first suggested by [16]. The authors proposed to follow the success of CNN backbones in extracting visual features from images and apply them for regressing the pose directly from the input image. Specifically, an MLP head was attached to a GoogLeNet backbone, regressing the position and orientation of the camera (replacing the classifier heads in the original architecture). This novel approach, albeit far less accurate than localization pipelines, enabled performing pose estimation with a single forward pass in only a few milliseconds.

To the best of our knowledge, the paradigm of regressing the camera pose from the final output of a CNN backbone was adopted by all regressors to date [30]. Variations to the architecture focused on alternatives to the original proposed

CNN backbone [20, 21, 38, 31] and on deeper, branching architectures for the MLP head [38, 21]. Other works tried to address overfitting by averaging over predictions from models with randomly dropped activations [14] or by reducing the dimensionality of the global image encoding with Long-Short-Term-Memory (LSTM) layers [36]. Multi-modality fusion (for example, with inertial sensors) was also suggested as a means to improve accuracy [5]. Recently, Wang et al. suggested to use attention in order to guide the regression process [37]. The authors applied dot product self-attention with SoftMax on the final output of the CNN backbone and updated it with the new attention-based representation (through summation), before regressing the pose with an MLP head. While our work also uses attention, we propose a novel paradigm, where instead of directly regressing the pose from a single global embedding (with/without attention-guided weights) multi-resolution activations maps are processed as a sequence of features using Transformer encoders.

In terms of the learning process, one of the main challenges is to appropriately weight the losses associated with the position and orientation predictions. Kendall et al. suggested to learn the parameters controlling the tradeoff between the losses to gain better performance [15]. This formulation was adopted by many pose regressors, however it still requires manually tuning the parameters’ initialization for different datasets [34]. In a recent work [31], the authors trained the model separately for position and orientation in order to reduce the need of additional parameters, while achieving comparable accuracy. Alternative representations for the orientation were also proposed to gain better balance and stability of the pose loss [38, 5]. As part of studying the performance of pose regressors, Sattler et al. proposed an IR-based baseline for camera pose regression [29]. With this baseline, pose predictions are made by taking a weighted average of poses from a set of nearest neighbors. The weighting is computed during inference time based on the distances between the IR encoding of the query and its neighbors. This baseline was used as an empirical illustration for some of the limitations of current pose regressors since no regressor was able to consistently surpass it on either outdoor or indoor datasets (we use the same datasets for evaluating our work).

Brachmann and Rother introduced a novel class of pose regression schemes [3, 4], by training a CNN to estimate the 3D locations corresponding to the pixels in the query image. This establishes 2D-3D correspondences that are utilized by a differentiable PnP-RANSAC to estimate the camera pose, in both training and testing phases. Such approaches achieve state-of-the-art accuracy. However, since PnP-RANSAC is applied at inference time, they are significantly slower compared to purely regression-based approaches. A different, yet related body of works, esti-

mate the absolute camera pose using the relative motion between the query image and a reference image, for which the ground truth pose is known. The learning thus focuses on regressing the relative pose given a pair of images [2, 17, 9]. These methods can generalize better since the model is no longer confined to the absolute reference scene, but require the availability of a pose-labelled database of anchors during inference time. Combining relative and absolute regression was also shown to achieve impressive accuracy [34, 25].

## 2.2. Attention and Transformers in Image Analysis

Transformers were introduced by Vaswani et al. [35] as a novel formulation of attention-based sequence encoding and analysis. Attention mechanisms [1] are neural network layers that aggregate information from the entire input sequence. Transformers introduced attention layers, that scan through each element of a sequence and update it by aggregating information from the whole sequence. Attention-based approaches were shown to outperform RNNs in encoding long sequences, and were applied in multiple recent works in natural language processing (NLP) and computer vision [8, 24]. In particular, in the context of image analysis, the use of attention relates to the bilinear pooling approach of Zhang et al. [39], and its multiple extensions [12]. These schemes compute the inner products between all CNN activations, and were shown to improve fine-grained recognition significantly. Bilinear pooling and attention schemes allow to implement ‘a needle in a haystack’ approaches, where each entry in the CNN activations map is adaptively weighted. Thus, allowing to numerically emphasize the contribution of the task-informative image locations, in contrast to the visual clutter. For instance, consider the attention weights visualization in Fig. 1, where we highlight the position and orientation of informative image locations. In this work, we utilize *self-attention* where the inner products are computed between the different entries of each particular activation map. This is implemented by an *Transformer encoder*, in contrast to using a *Transformer decoder* where the inner products between the input data and an additional set of vectors, denoted as *queries*, are computed.

## 3. Transformer Encoder for Pose Regression

In this work we propose to localize a camera by estimating  $\mathbf{p} = \langle \mathbf{x}, \mathbf{q} \rangle$ , where  $\mathbf{x} \in \mathbb{R}^3$  is the position of the camera in the world and  $\mathbf{q} \in \mathbb{R}^4$  is the quaternion encoding its 3D orientation. Thus, the problem of camera pose regression is to jointly learn two regression tasks: regressing the camera position  $\mathbf{x}$  and regressing the camera orientation  $\mathbf{q}$ . We model each task as a sequence-to-one problem, where the input is a sequential representation of a learned activation map and the output is an estimate of the corresponding pose component (either  $\mathbf{x}$  or  $\mathbf{q}$ ). Follow-

ing the success of Transformers in learning sequence-to-one and sequence-to-sequence problems in NLP [24] and more recently in Computer Vision [7], we propose to use Transformer encoders for aggregating sequential representations into a single latent vector. Specifically, we employ positional and orientational encoders that learn to emphasize the visual cues for position and orientation inference, respectively. An MLP can then regress the resulting encoder output, replacing the classifier head used in standard sequence-to-one architectures [8]. We denote our model *TransPoseNet* as it shifts from the conventional pose regression paradigm to a Transformer-based model. An overview of the proposed scheme is shown in Fig. 1, where the image is initially processed by a CNN backbone to compute activation maps that are analyzed by the dual encoders and corresponding regression heads.

### 3.1. Network Architecture

**TransPoseNet** is composed of a shared convolutional backbone and two branches for separately regressing the position and orientation of the camera. Each branch consists of a separate Transformer encoder and an MLP head. Using separate activation maps and Transformers allows us to attend to the different features at different resolutions depending on the particular learned task.

**Convolutional Backbone.** The activation maps of convolutional backbones capture latent visual features at different resolutions. Given an image  $\mathbf{I} \in \mathbb{R}^{H \times W \times C}$ , we sample the backbone at two different resolutions and take an activation map per regression task:  $M_x$  and  $M_q$  respectively.

**Sequential Representations of Activation Maps.** We follow [7] and convert an activation map  $\mathbf{M} \in \mathbb{R}^{H_m \times W_m \times C_m}$  to a sequence  $\widehat{\mathbf{M}} \in \mathbb{R}^{H_m \cdot W_m \times C_t}$  using a  $1 \times 1$  convolution (projecting to dimension  $C_t$ ) followed by flattening. We further append a learned *orientation/position token*  $\mathbf{t} \in \mathbb{R}^{C_t}$  to the sequence of map features, analogous to the *class token* in sequence-to-one NLP classification Transformer architectures [8]. Hence, the input to the encoder is given by:

$$E_{in} = [\mathbf{t}, \widehat{\mathbf{M}}] \in \mathbb{R}^{(H_m \cdot W_m + 1) \times C_t}. \quad (1)$$

**Positional Encoding.** In order to preserve the spatial information of each location in the map, and assign a particular positional encoding to the token  $\mathbf{t}$ , the spatial positions are encoded using positional encoding as in [7]. We train two one-dimensional encodings for the  $X$  and  $Y$  axes separately, to reduce the number of learnt positional parameters. Thus, for an activation map  $\mathbf{M}$  we define the sets of positional embedding vectors  $\mathbf{E}_x \in \mathbb{R}^{(W_m+1) \times C_t/2}$  and  $\mathbf{E}_y \in \mathbb{R}^{(H_m+1) \times C_t/2}$ , such that a spatial position  $(i, j)$ ,  $i \in 1..H_m, j \in 1..W_m$ , is encoded by the concatenating of

the corresponding embedding vector:

$$\mathbf{E}_{pos}^{i,j} = \begin{bmatrix} \mathbf{E}_x^j \\ \mathbf{E}_y^i \end{bmatrix} \in \mathbb{R}^{C_t}. \quad (2)$$

The pose token is assigned with position  $(0, 0)$  and the embedding vectors  $(\mathbf{E}_x^0, \mathbf{E}_y^0)$ , as these vectors will only be associated with that token. Similar to the activation map  $\mathbf{M}$ , the positional embeddings are reshaped as sequence  $\widehat{\mathbf{E}} \in \mathbb{R}^{(H_m \cdot W_m + 1) \times C_t}$  and passed to the encoder.

**Transformer Encoder.** We use a standard Transformer encoder architecture [8] consisting of  $n$  identical blocks. Each block contains a self multi-head attention (MHA) module and an MLP with two layers and gelu non-linearity. The input is passed through a LayerNorm [35] before each module (MHA/MLP) and added back to the output with residual connections [35] and dropout. As in [7] we add the position encoding to the input before each layer and normalize the output of the final layer with an additional LN pass. The encoder's output  $\mathbf{t}' \in \mathbb{R}^{C_t}$  at the position of the special token  $t$ , represents a global and context aware summarization of the local features of the input activation map.

**MLP Head.** an MLP head with one hidden layer and gelu non-linearity regresses the target vector ( $\mathbf{x}$  or  $\mathbf{q}$ ) from  $\mathbf{t}'$ .

### 3.2. Camera Pose Loss

Camera pose regressors are optimized to minimize the deviation between the ground truth pose  $\mathbf{p}_0 = \langle \mathbf{x}_0, \mathbf{q}_0 \rangle$  and the predicted pose  $\mathbf{p} = \langle \mathbf{x}, \mathbf{q} \rangle$ . The position loss  $L_x$  and the orientation loss  $L_q$  are measured by the Euclidean distance between the ground truth and the estimation:

$$L_x = \|\mathbf{x}_0 - \mathbf{x}\|_2 \quad (3)$$

$$L_q = \left\| \mathbf{q}_0 - \frac{\mathbf{q}}{\|\mathbf{q}\|} \right\|_2 \quad (4)$$

where  $\mathbf{q}$  is normalized to unit vector in order to map to a valid rotation matrix. In order to balance between the two losses, while considering their scale differences, Kendall et al. suggested to learn their relative weight by modelling the uncertainty of each task [15]:

$$L_p = L_x \exp(-s_x) + s_x + L_q \exp(-s_q) + s_q, \quad (5)$$

where  $s_x$  and  $s_q$  are learned parameters. Recently, Shavit and Ferens showed the advantage of separately learning each task on its own [31]. Here, we follow a combined approach, where we first train the entire model to minimize Eq. 5 and then fine-tune each MLP head solely with its respective loss (Eqs. 3 and 4).

### 3.3. Implementation Details

Our localization approach is implemented using EfficientNet-B0 [33] as our convolutional backbone, previously shown to focus on informative visual features for image classification. The EfficientNet backbone has several reduction levels, each corresponding to activation maps with decreasing resolution and increasing depth. We use an open source implementation of EfficientNet [19] and use the activation maps from two endpoints (reduction levels):  $m_{rdct4} \in \mathbb{R}^{14 \times 14 \times 112}$  and  $m_{rdct3} \in \mathbb{R}^{28 \times 28 \times 40}$ . We use  $m_{rdct4}$  and  $m_{rdct3}$  as inputs for the position and orientation branches, respectively. We linearly project each activation map to a common depth dimension  $C_t = 256$ , and learn positional encoding of the same depth. For the Transformer encoder we use a standard implementation with six blocks and a dropout of  $p = 0.1$ . Each block contains an MHA layer with four heads and an MLP preserving the input dimension  $C_t$ . The hidden layer of the MLP regressor heads expands the dimension from 256 to 1024 before regressing the output vector with a fully connected layer.

## 4. Experimental Results

Our proposed scheme focuses on improving the accuracy of *absolute pose regression*. As such, we evaluate it on multiple contemporary datasets used for benchmarking camera pose regressors, and compare the results to recent state-of-the-art regression-based absolute localization methods. Other classes of localization schemes, described in section 2.1, which utilize additional data at inference time (localization pipelines [32, 26, 22, 10] and relative pose regression [2, 17, 9]) or that are an order of magnitude slower (3D-based scene coordinate regression [3, 4]) are not considered for this analysis.

**Datasets.** The Cambridge Landmarks [16] dataset depicts an urban environment and represents outdoor localization tasks with a spatial extent of  $\sim 900 - 5500m^2$ . We use four of its six scenes for comparative evaluation, as the other two scenes are not commonly benchmarked. The 7Scenes [13] dataset includes seven small-scale indoor scenes, depicting a spatial extent of  $\sim 1 - 10m^2$ . Both datasets present various localization challenges such as occlusions, reflections, motion blur, lighting conditions, repetitive textures and variations in view point and trajectory.

**Training.** We optimize our model using Adam, with  $\beta_1 = 0.9$ ,  $\beta_2 = 0.999$  and  $\epsilon = 10^{-10}$  and a batch size of 8. At the first step of the training we minimize the loss defined in Eq. 5. Loss parameters are initialized as in [34]. We use a learning rate of  $\lambda = 10^{-4}$  and decrease it by a factor of 10 every 100 (200) epochs for indoor (outdoor) localization for up to 300 (600) epochs. We apply a weight decay of  $10^{-4}$  and train the encoders with a dropout  $p = 0.1$ . At the second training stage, we fine-tune each MLP head separately

with its respective loss (Eqs. 3 and 4), while freezing all other weights in the network. This allows us to achieve better performance without needing to trade-off between the two objectives. Since the position is dominant in localizing large scale scenes, we fine-tune the orientation head with a latent position prior from the position Transformer encoder (changing the orientation MLP to take a concatenated input). For indoor localization, we train both heads independently and use a higher learning rate and a higher weight decay ( $10^{-3}$  and  $10^{-2}$ , respectively). In order to allow our model to better generalize, we follow the augmentation procedure used by [16]. At train time we rescale the image so that its smaller edge is resized to 256 pixels and take a random  $224 \times 224$  crop. We then randomly jitter the brightness, contrast and saturation. At test time we take the center crop after rescaling with no further augmentations. All models were trained on a single NVIDIA Tesla V100 GPU using the PyTorch framework [23].

### 4.1. Comparative Analysis of Camera Pose Regressors

**Outdoor Localization.** We report the median position and orientation errors on four outdoor scenes from the Cambridge Landmarks dataset. Table 1 shows the localization results of our method (TransPoseNet) compared to all other pose regressors reporting on this benchmark using a single input image. We also include the results of an IR baseline recently proposed as a reference for evaluating the limitations of absolute pose regression methods [29]. TransPoseNet yields the lowest position error across all scenes and provides the lowest orientation error when evaluated on the Shop Facade scene. It also achieves the highest number of *state-of-the-art* results across the dataset. When summarizing the results (Table 2), TransPoseNet is the only regressor achieving sub-meter accuracy. It ranks first in terms of average position error and third in orientation. In addition, when considering the total rank (average of position and orientation ranks), TransPoseNet again ranks first.

We also consider an IR baseline, recently shown to present a lower error bound on the performance of current pose regressors. Figures 2a and 2b compare the position and orientation errors of different pose regressors with respect to the IR baseline results (indicated in black). TransPoseNet is the only pose regressor whose localization error is consistently below the IR error bar, across both position and orientation. To the best of our knowledge, TransPoseNet is the only pose regressor to-date to achieve this result.

**Indoor Localization.** Table 3 shows the results obtained when evaluating TransPoseNet on the 7Scenes dataset. As in outdoor localization we compare its performance to all pose regressors reporting on this benchmark with a single image input. TransPoseNet achieves the best positional error in six out of the seven scenes and the highest number of

**Table 1:** Comparative analysis of pose regressors on the Cambridge Landmarks dataset (outdoor localization). We report the median position/orientation error in meters/degrees for each method. Best results are highlighted in bold.

| Method                     | K. College        | Old Hospital      | Shop Facade      | St. Mary          |
|----------------------------|-------------------|-------------------|------------------|-------------------|
| IR Baseline [29]           | 1.48/4.45         | 2.68/4.63         | 0.90/4.32        | 1.62/6.06         |
| PoseNet [16]               | 1.92/5.40         | 2.31/5.38         | 1.46/8.08        | 2.65/8.48         |
| BayesianPN [14]            | 1.74/4.06         | 2.57/5.14         | 1.25/7.54        | 2.11/8.38         |
| LSTM-PN [36]               | 0.99/3.65         | 1.51/4.29         | 1.18/7.44        | 1.52/6.68         |
| SVS-Pose [21]              | 1.06/2.81         | 1.50/4.03         | 0.63/5.73        | 2.11/8.11         |
| GPoseNet [6]               | 1.61/2.29         | 2.62/3.89         | 1.14/5.73        | 2.93/6.46         |
| PoseNet-Learnable [15]     | 0.99/1.06         | 2.17/ <b>2.94</b> | 1.05/3.97        | 1.49/3.43         |
| GeoPoseNet [15]            | 0.88/ <b>1.04</b> | 3.20/3.29         | 0.88/3.78        | 1.57/ <b>3.32</b> |
| MapNet [5]                 | 1.07/1.89         | 1.94/3.91         | 1.49/4.22        | 2.00/4.53         |
| IRPNet [31]                | 1.18/2.19         | 1.87/3.38         | 0.72/3.47        | 1.87/4.94         |
| <b>TransPoseNet (Ours)</b> | <b>0.60/2.43</b>  | <b>1.45/3.08</b>  | <b>0.55/3.49</b> | <b>1.09/4.99</b>  |

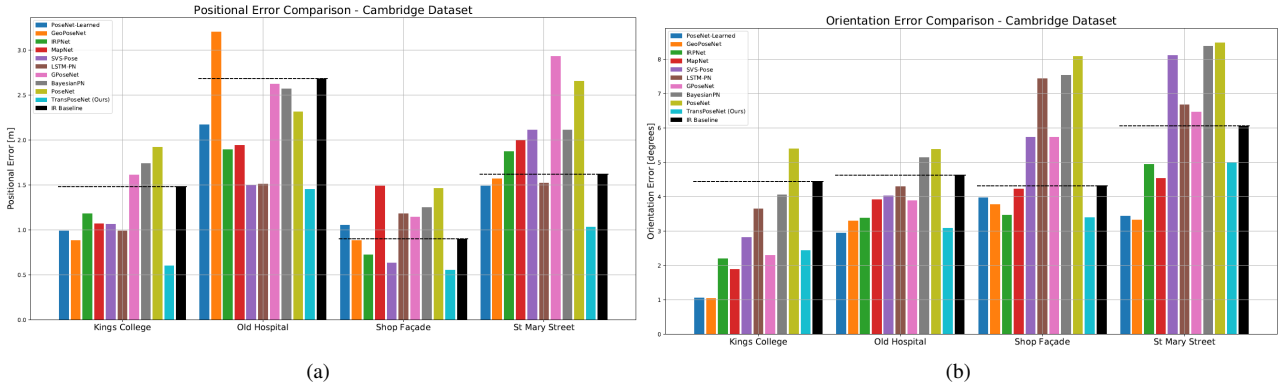


**Figure 2:** Visual comparison of position (a) and orientation (b) errors of different pose regressors, with respect to the IR baseline reported by [29]. The results are reported for the Cambridge Landmarks dataset.

**Table 2:** Localization results for the Cambridge Landmarks dataset. We report the average position/orientation errors in meters/degrees and the respective rankings. Best results are highlighted in bold. The final ranking is set according to the average rank.

| Method                     | Average [m/deg]   | Ranks       | Final Rank |
|----------------------------|-------------------|-------------|------------|
| PoseNet [16]               | 2.09/6.84         | 10/10       | 10         |
| BayesianPN [14]            | 1.92/6.28         | 8/9         | 9          |
| LSTM-PN [36]               | 1.30/5.52         | 2/8         | 5          |
| SVS-Pose [21]              | 1.33/5.17         | 3/7         | 5          |
| GPoseNet [6]               | 2.08/4.59         | 9/6         | 8          |
| PoseNet-Learnable [15]     | 1.43/ <b>2.85</b> | 5/ <b>1</b> | 2          |
| GeoPoseNet [15]            | 1.63/2.86         | 6/2         | 3          |
| MapNet [5]                 | 1.63/3.64         | 6/5         | 7          |
| IRPNet [31]                | 1.42/3.45         | 4/4         | 3          |
| <b>TransPoseNet (Ours)</b> | <b>0.91/3.47</b>  | <b>1/3</b>  | <b>1</b>   |

*state-of-the-art* results overall. Similar to outdoor localization, TransPoseNet ranks favorably in terms of position and orientation errors, achieving first and second place respectively and ranking first in total (Table 4). Another attention-based method [37] also achieves the first place in total ranking, but with fewer *state-of-the-art* results (two versus seven achieved with TransPoseNet). When comparing the performance to the IR baseline (Table 3), TransPoseNet has 14 out of 15 results under the bar, more than any other pose regressor to-date.

## 4.2. Paying Attention to Local Features

A key element in our proposed method is the use of one encoder per task (position and orientation) for processing activation maps. The motivation behind this design is to allow each encoder to attend to different features in the image. We assume that the network will focus on features such as corners and blobs to estimate the relative translation, and on edges and lines for estimating the relative rotation. Figure 3 shows attention heatmaps for three query



**Table 3:** Comparative analysis of pose regressors on the 7Scenes dataset (indoor localization). We report the median position/orientation error in meters/degrees for each method. Best results are highlighted in bold.

| Method                     | Chess             | Fire              | Heads             | Office            | Pumpkin          | Kitchen           | Stairs            |
|----------------------------|-------------------|-------------------|-------------------|-------------------|------------------|-------------------|-------------------|
| IR Baseline [29]           | 0.18/10.0         | 0.33/12.4         | 0.15/14.3         | 0.25/10.1         | 0.26/9.42        | 0.27/11.1         | <b>0.24</b> /14.7 |
| PoseNet [16]               | 0.32/8.12         | 0.47/14.4         | 0.29/12.0         | 0.48/7.68         | 0.47/8.42        | 0.59/8.64         | 0.47/13.8         |
| BayesianPN [14]            | 0.37/7.24         | 0.43/13.7         | 0.31/12.0         | 0.48/8.04         | 0.61/7.08        | 0.58/7.54         | 0.48/13.1         |
| LSTM-PN [36]               | 0.24/5.77         | 0.34/11.9         | 0.21/13.7         | 0.30/8.08         | 0.33/7.0         | 0.37/8.83         | 0.40/13.7         |
| GPoseNet [6]               | 0.20/7.11         | 0.38/12.3         | 0.21/13.8         | 0.28/8.83         | 0.37/6.94        | 0.35/8.15         | 0.37/12.5         |
| PoseNet-Learnable [15]     | 0.14/4.50         | 0.27/11.8         | 0.18/12.1         | 0.20/5.77         | 0.25/4.82        | 0.24/5.52         | 0.37/10.6         |
| GeoPoseNet [15]            | 0.13/4.48         | 0.27/11.3         | 0.17/13.0         | 0.19/5.55         | 0.26/4.75        | 0.23/5.35         | 0.35/12.4         |
| MapNet [5]                 | <b>0.08/3.25</b>  | 0.27/11.7         | 0.18/13.3         | <b>0.17/5.15</b>  | 0.22/4.02        | 0.23/4.93         | 0.30/12.1         |
| IRPNet [31]                | 0.13/5.64         | 0.25/9.67         | 0.15/13.1         | 0.24/6.33         | 0.22/5.78        | 0.30/7.29         | 0.34/11.6         |
| AttLoc [37]                | 0.10/4.07         | 0.25/11.4         | 0.16/11.8         | <b>0.17</b> /5.34 | 0.21/4.37        | 0.23/5.42         | 0.26/10.5         |
| <b>TransPoseNet (Ours)</b> | <b>0.08</b> /5.68 | <b>0.24</b> /10.6 | <b>0.13</b> /12.7 | <b>0.17</b> /6.34 | <b>0.17</b> /5.6 | <b>0.19</b> /6.75 | 0.30/ <b>7.02</b> |

**Table 4:** Localization results for the 7Scenes dataset. We report the average position/orientation errors in meters/degrees and the respective rankings. Best results are highlighted in bold. The final ranking is set according to the average rank.

| Method                     | Average [m/deg]   | Ranks | Final Rank |
|----------------------------|-------------------|-------|------------|
| PoseNet [16]               | 0.44/10.4         | 9/10  | 10         |
| BayesianPN [14]            | 0.47/9.81         | 10/7  | 9          |
| LSTM-PN [36]               | 0.31/9.86         | 7/8   | 7          |
| GPoseNet [6]               | 0.31/9.95         | 7/9   | 8          |
| PoseNet-Learnable [15]     | 0.24/7.87         | 6/4   | 5          |
| GeoPoseNet [15]            | 0.23/8.12         | 4/5   | 4          |
| MapNet [5]                 | 0.21/7.78         | 3/2   | 3          |
| IRPNet [31]                | 0.23/8.49         | 4/6   | 5          |
| AttLoc [37]                | 0.20/7.56         | 2/1   | 1          |
| <b>TransPoseNet (Ours)</b> | <b>0.18</b> /7.78 | 1/2   | 1          |

images taken from different scenes in the Cambridge Landmarks and the 7Scenes datasets. Each row depicts the query image and the upsampled attention weights taken from the last layers of the position and orientation encoders (second and third column, respectively). The position encoder tends to assign higher weights to features that are intuitively more distinctive for coarser localization and position estimation. In contrast, the orientation encoder focuses on lines and long edges that are informative for estimating the rotational motion. For example, consider the triplet in the third row, the position encoder focuses on the windows at the image’s center of mass, while the orientation encoder attends to the elongated spires. The observed differences between the two encoders reinforces our dual-head model architecture. The relative motion emerging from attention-driven local features in the image, with respect to a memorized map, can be summarized with context-aware global absolute image descriptors used for regressing the position and orientation.

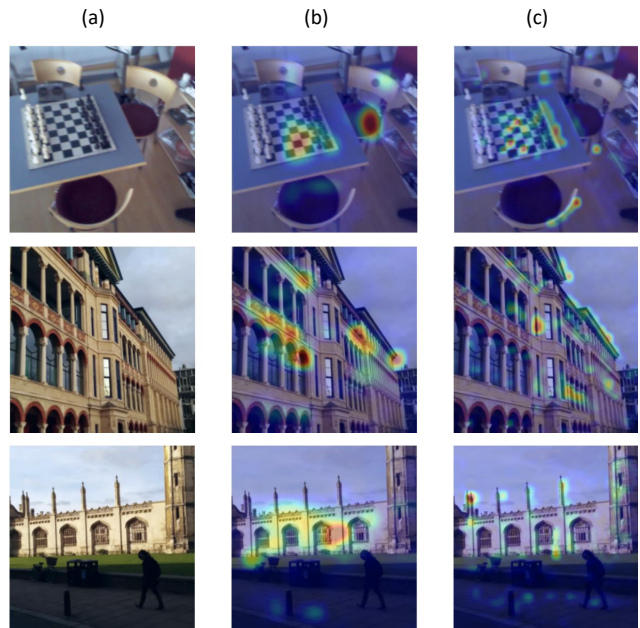


**Figure 3:** Heatmap visualization of attention weights from the position and orientation encoders (column (b) and (c)). Each row shows the query image (column (a)) along with the respective attentional heatmaps.

### 4.3. Ablation Study

We study the importance and impact of two aspects of our model design: the attention mechanism and the resolution and depth of the activation maps. In each evaluation, we started from the network used in Section 4.1 and modified a *single* algorithmic component or hyper-parameter. All ablations were conducted using the Shop Facade scene.

**Backbone.** For studying the choice of backbone, we considered the Resnet50, EfficientNetB0 and Efficient-

**Table 5:** Ablation study of CNN backbones evaluated on the Shop Facade scene. We report the median position and orientation errors. Both EfficientNet-based CNNs outperform the Resnet50 CNN. Using the EfficientNetB1 backbone degrades the accuracy due to overfitting.

| Backbone              | Position<br>[meters] | Orientation<br>[degrees] |
|-----------------------|----------------------|--------------------------|
| Resnet50              | 0.81                 | 4.76                     |
| <b>EfficientNetB0</b> | <b>0.65</b>          | <b>3.63</b>              |
| EfficientNetB1        | 0.69                 | 4.03                     |

NetB1 CNNs, where both EfficientNet variants use significantly less parameters than Resnet50. As shown in Table 5, both EfficientNet variants significantly outperforms Resnet50. It is unclear from our simulations, whether this is due to less overfitting or to their improved architecture. The smaller EfficientNetB0 backbone provides the best results.

**The Role of Attention and Transformers.** To study the parameters of the Transformer encoders, we trained our scheme with a varying number of Transformer encoder layers. On the hand, the more layers are used, the better the learning capacity. On the other hand, an over-parameterized Transformer encoder might lead to overfitting. The results reported in Table 6 show a ‘sweet spot’ when using six layers. We also varied the Transformer encoders’ inner embedding dimension to verify our choice. The results in Table 7 show that, similar to varying the number of layers, there exists a ‘sweet spot’ when using 256 for the encoder latent dimension.

**Table 6:** Ablations of the Transformer Encoder configuration evaluated on the Shop Facade scene. We report the median position and orientation errors. Using six layers optimizes the accuracy and avoids overfitting.

| #Encoder Layers | Position<br>[meters] | Orientation<br>[degrees] |
|-----------------|----------------------|--------------------------|
| 2               | 0.92                 | 4.61                     |
| 4               | 0.93                 | 4.2                      |
| <b>6</b>        | <b>0.65</b>          | <b>3.63</b>              |
| 8               | 0.89                 | 3.75                     |

**Localizing with Coarse and Fine Activation Maps.** Activation maps from different endpoints of a CNN backbone capture different features in the input image. Deeper reduction levels cover growing areas in the figure with an increased depth. As orientation and position estimation may require different feature complexity, we train our model with different combinations of  $m_{rdct3} \in \mathbb{R}^{28 \times 28 \times 40}$  and  $m_{rdct4} \in \mathbb{R}^{14 \times 14 \times 112}$  from the EfficientNet backbone, as inputs for the position and orientation encoders (without fine-tuning). Table 8 shows the results of four combinations

**Table 7:** Ablations of model’s embedding dimensionality, evaluated on the Shop Facade scene. We report the median position and orientation errors.

| Encoder Dimension | Position<br>[meters] | Orientation<br>[degrees] |
|-------------------|----------------------|--------------------------|
| 64                | 0.79                 | 4.35                     |
| 128               | 0.81                 | 3.99                     |
| <b>256</b>        | <b>0.65</b>          | <b>3.63</b>              |
| 512               | 0.68                 | 4.18                     |

evaluated on the Shop Facade scene from the Cambridge Landmarks dataset. We either provide  $m_{rdct4}/m_{rdct3}$  to both encoder heads or use a combination (providing  $m_{rdct3}$  to one encoder and  $m_{rdct4}$  to the other). Assigning the position encoder with coarser activation maps yields better accuracy. An opposite trend is observed for activation maps used by the orientation encoder.

**Table 8:** Ablations of activation maps evaluated on the Shop Facade scene. We provide different combinations of  $m_{rdct3} \in \mathbb{R}^{28 \times 28 \times 40}$  and  $m_{rdct4} \in \mathbb{R}^{14 \times 14 \times 112}$  to the encoder heads and report the median position and orientation errors.

| Reduction<br>Position/Orientation       | Position<br>[meters] | Orientation<br>[degrees] |
|---|----------------------|--------------------------|
| $m_{rdct3}/m_{rdct3}$                   | 1.08                 | 3.60                     |
| $m_{rdct3}/m_{rdct4}$                   | 0.99                 | 4.32                     |
| <b><math>m_{rdct4}/m_{rdct3}</math></b> | <b>0.65</b>          | <b>3.63</b>              |
| $m_{rdct4}/m_{rdct4}$                   | 0.81                 | 4.05                     |

## 5. Conclusion

We presented a novel paradigm for camera pose regression which uses sequential representations of multi-scale activation maps instead of a single global descriptor from a CNN backbone. By applying dual multi-head attention encoders, our model is able to focus on different local features depending on the learned task. Our method ranks first on both outdoor and indoor benchmarks and achieves a more consistent performance with respect to recent baselines.

## References

- [1] Dzmitry Bahdanau, Kyunghyun Cho, and Yoshua Bengio. Neural machine translation by jointly learning to align and translate. In Yoshua Bengio and Yann LeCun, editors, *3rd International Conference on Learning Representations, ICLR 2015, San Diego, CA, USA, May 7-9, 2015, Conference Track Proceedings*, 2015.
- [2] Vassileios Balntas, Shuda Li, and Victor Prisacariu. Relocnet: Continuous metric learning relocalisation using neural nets. In *Proceedings of the European Conference on Computer Vision (ECCV)*, September 2018.



- [3] E. Brachmann, A. Krull, S. Nowozin, J. Shotton, F. Michel, S. Gumhold, and C. Rother. Dsac – differentiable ransac for camera localization. In *2017 IEEE Conference on Computer Vision and Pattern Recognition (CVPR)*, pages 2492–2500, Los Alamitos, CA, USA, jul 2017. IEEE Computer Society.
- [4] E. Brachmann and C. Rother. Learning less is more - 6d camera localization via 3d surface regression. In *2018 IEEE/CVF Conference on Computer Vision and Pattern Recognition*, pages 4654–4662, 2018.
- [5] Samarth Brahmabhatt, Jinwei Gu, Kihwan Kim, James Hays, and Jan Kautz. Geometry-aware learning of maps for camera localization. In *IEEE Conference on Computer Vision and Pattern Recognition (CVPR)*, 2018.
- [6] Ming Cai, Chunhua Shen, and Ian Reid. A hybrid probabilistic model for camera relocalization. 2019.
- [7] Nicolas Carion, Francisco Massa, Gabriel Synnaeve, Nicolas Usunier, Alexander Kirillov, and Sergey Zagoruyko. End-to-end object detection with transformers. In Andrea Vedaldi, Horst Bischof, Thomas Brox, and Jan-Michael Frahm, editors, *Computer Vision – ECCV 2020*, pages 213–229, Cham, 2020. Springer International Publishing.
- [8] Jacob Devlin, Ming-Wei Chang, Kenton Lee, and Kristina Toutanova. BERT: Pre-training of deep bidirectional transformers for language understanding. In *Proceedings of the 2019 Conference of the North American Chapter of the Association for Computational Linguistics: Human Language Technologies, Volume 1 (Long and Short Papers)*, pages 4171–4186, Minneapolis, Minnesota, June 2019. Association for Computational Linguistics.
- [9] Mingyu Ding, Zhe Wang, Jiankai Sun, Jianping Shi, and Ping Luo. Camnet: Coarse-to-fine retrieval for camera relocalization. In *Proceedings of the IEEE/CVF International Conference on Computer Vision (ICCV)*, October 2019.
- [10] M. Dusmanu, I. Rocco, T. Pajdla, M. Pollefeys, J. Sivic, A. Torii, and T. Sattler. D2-net: A trainable cnn for joint description and detection of local features. In *2019 IEEE/CVF Conference on Computer Vision and Pattern Recognition (CVPR)*, pages 8084–8093, 2019.
- [11] Martin A. Fischler and Robert C. Bolles. Random sample consensus: A paradigm for model fitting with applications to image analysis and automated cartography. *Commun. ACM*, 24(6):381–395, June 1981.
- [12] Y. Gao, O. Beijbom, N. Zhang, and T. Darrell. Compact bilinear pooling. In *2016 IEEE Conference on Computer Vision and Pattern Recognition (CVPR)*, pages 317–326, 2016.
- [13] B. Glocker, S. Izadi, J. Shotton, and A. Criminisi. Real-time rgb-d camera relocalization. In *2013 IEEE International Symposium on Mixed and Augmented Reality (ISMAR)*, pages 173–179, 2013.
- [14] Alex Kendall and Roberto Cipolla. Modelling uncertainty in deep learning for camera relocalization. In *Proceedings of the International Conference on Robotics and Automation (ICRA)*, 2016.
- [15] A. Kendall and R. Cipolla. Geometric loss functions for camera pose regression with deep learning. In *2017 IEEE Conference on Computer Vision and Pattern Recognition (CVPR)*, pages 6555–6564, 2017.
- [16] A. Kendall, M. Grimes, and R. Cipolla. PoseNet: A convolutional network for real-time 6-dof camera relocalization. In *2015 IEEE International Conference on Computer Vision (ICCV)*, pages 2938–2946, 2015.
- [17] Z. Laskar, I. Melekhov, S. Kalia, and J. Kannala. Camera relocalization by computing pairwise relative poses using convolutional neural network. In *2017 IEEE International Conference on Computer Vision Workshops (ICCVW)*, pages 920–929, 2017.
- [18] David G. Lowe. Distinctive image features from scale-invariant keypoints. *Int. J. Comput. Vision*, 60(2):91–110, Nov. 2004.
- [19] Luke Melaskeyriazi. efficientnet-pytorch. <https://pypi.org/project/efficientnet-pytorch/>, 2019.
- [20] Iaroslav Melekhov, Juha Ylioinas, Juho Kannala, and Esa Rahtu. Image-based localization using hourglass networks. In *2017 IEEE International Conference on Computer Vision Workshops, ICCV Workshops 2017, Venice, Italy, October 22-29, 2017*, pages 870–877. IEEE Computer Society, 2017.
- [21] Tayyab Naseer and W. Burgard. Deep regression for monocular camera-based 6-dof global localization in outdoor environments. *2017 IEEE/RSJ International Conference on Intelligent Robots and Systems (IROS)*, pages 1525–1530, 2017.
- [22] H. Noh, A. Araujo, J. Sim, T. Weyand, and B. Han. Large-scale image retrieval with attentive deep local features. In *2017 IEEE International Conference on Computer Vision (ICCV)*, pages 3476–3485, 2017.
- [23] Adam Paszke, Sam Gross, Francisco Massa, Adam Lerer, James Bradbury, Gregory Chanan, Trevor Killeen, Zeming Lin, Natalia Gimelshein, Luca Antiga, Alban Desmaison, Andreas Kopf, Edward Yang, Zachary DeVito, Martin Raison, Alykhan Tejani, Sasank Chilamkurthy, Benoit Steiner, Lu Fang, Junjie Bai, and Soumith Chintala. Pytorch: An imperative style, high-performance deep learning library. In H. Wallach, H. Larochelle, A. Beygelzimer, F. Alche-Buc, E. Fox, and R. Garnett, editors, *Advances in Neural Information Processing Systems*, volume 32, pages 8026–8037. Curran Associates, Inc., 2019.
- [24] Alec Radford, Jeff Wu, Rewon Child, David Luan, Dario Amodei, and Ilya Sutskever. Language models are unsupervised multitask learners. 2019.
- [25] N. Radwan, A. Valada, and W. Burgard. Vlocnet++: Deep multitask learning for semantic visual localization and odometry. *IEEE Robotics and Automation Letters*, 3(4):4407–4414, 2018.
- [26] P. Sarlin, C. Cadena, R. Siegwart, and M. Dymczyk. From coarse to fine: Robust hierarchical localization at large scale. In *2019 IEEE/CVF Conference on Computer Vision and Pattern Recognition (CVPR)*, pages 12708–12717, 2019.
- [27] Paul-Edouard Sarlin, Daniel DeTone, Tomasz Malisiewicz, and Andrew Rabinovich. Superglue: Learning feature matching with graph neural networks. In *Proceedings of the IEEE/CVF Conference on Computer Vision and Pattern Recognition*, pages 4938–4947, 2020.
- [28] T. Sattler, B. Leibe, and L. Kobbelt. Efficient effective prioritized matching for large-scale image-based localization.

*IEEE Transactions on Pattern Analysis and Machine Intelligence*, 39(9):1744–1756, 2017.

- [29] T. Sattler, Q. Zhou, M. Pollefeys, and L. Leal-Taixé. Understanding the limitations of cnn-based absolute camera pose regression. In *2019 IEEE/CVF Conference on Computer Vision and Pattern Recognition (CVPR)*, pages 3297–3307, 2019.
- [30] Yoli Shavit and Ron Ferens. Introduction to camera pose estimation with deep learning, 2019.
- [31] Yoli Shavit and Ron Ferens. Do we really need scene-specific pose encoders. In *To Appear in 2021 IEEE International Conference on Pattern Recognition (ICPR)*, 2021.
- [32] H. Taira, M. Okutomi, T. Sattler, M. Cimpoi, M. Pollefeys, J. Sivic, T. Pajdla, and A. Torii. Inloc: Indoor visual localization with dense matching and view synthesis. *IEEE Transactions on Pattern Analysis and Machine Intelligence*, pages 1–1, 2019.
- [33] Mingxing Tan and Quoc Le. EfficientNet: Rethinking model scaling for convolutional neural networks. volume 97 of *Proceedings of Machine Learning Research*, pages 6105–6114, Long Beach, California, USA, 09–15 Jun 2019. PMLR.
- [34] Abhinav Valada, Noha Radwan, and Wolfram Burgard. Deep auxiliary learning for visual localization and odometry. *ICRA*, pages 6939–6946, 2018.
- [35] Ashish Vaswani, Noam Shazeer, Niki Parmar, Jakob Uszkoreit, Llion Jones, Aidan N Gomez, Łukasz Kaiser, and Illia Polosukhin. Attention is all you need. In I. Guyon, U. V. Luxburg, S. Bengio, H. Wallach, R. Fergus, S. Vishwanathan, and R. Garnett, editors, *Advances in Neural Information Processing Systems*, volume 30, pages 5998–6008. Curran Associates, Inc., 2017.
- [36] F. Walch, C. Hazirbas, L. Leal-Taixé, T. Sattler, S. Hilsenbeck, and D. Cremers. Image-based localization using lstms for structured feature correlation. In *2017 IEEE International Conference on Computer Vision (ICCV)*, pages 627–637, 2017.
- [37] Bing Wang, Changhao Chen, Chris Xiaoxuan Lu, Peijun Zhao, Niki Trigoni, and Andrew Markham. Atloc: Attention guided camera localization. In *Proceedings of the AAAI Conference on Artificial Intelligence*, volume 34, pages 10393–10401, 2020.
- [38] J. Wu, L. Ma, and X. Hu. Delving deeper into convolutional neural networks for camera relocation. In *2017 IEEE International Conference on Robotics and Automation (ICRA)*, pages 5644–5651, 2017.
- [39] X. Zhang, H. Xiong, W. Zhou, W. Lin, and Q. Tian. Picking deep filter responses for fine-grained image recognition. In *2016 IEEE Conference on Computer Vision and Pattern Recognition (CVPR)*, pages 1134–1142, 2016.